

# Surg-3M: A Dataset and Foundation Model for Perception in Surgical Settings

Chengan Che, Chao Wang, Tom Vercauteren, Sophia Tsoka, Luis C. Garcia-Peraza-Herrera  
King's College London, London, United Kingdom

{chengan.che, chao.wang, tom.vercauteren, sophia.tsoka, luis.c.garcia\_peraza\_herrera}@kcl.ac.uk

## Abstract

Advancements in computer-assisted surgical procedures heavily rely on accurate visual data interpretation from camera systems used during surgeries. Traditional open-access datasets focusing on surgical procedures are often limited by their small size, typically consisting of fewer than 100 videos with less than 100K images. To address these constraints, a new dataset called Surg-3M has been compiled using a novel aggregation pipeline that collects high-resolution videos from online sources. Featuring an extensive collection of over 4K surgical videos and more than 3 million high-quality images from multiple procedure types, Surg-3M offers a comprehensive resource surpassing existing alternatives in size and scope, including two novel tasks. To demonstrate the effectiveness of this dataset, we present SurgFM, a self-supervised foundation model pretrained on Surg-3M that achieves impressive results in downstream tasks such as surgical phase recognition, action recognition, and tool presence detection. Combining key components from ConvNeXt, DINO, and an innovative augmented distillation method, SurgFM exhibits exceptional performance compared to specialist architectures across various benchmarks. Our experimental results show that SurgFM outperforms state-of-the-art models in multiple downstream tasks, including significant gains in surgical phase recognition (+8.9pp, +4.7pp, and +3.9pp of Jaccard in AutoLaparo, M2CAI16, and Cholec80), action recognition (+3.1pp of mAP in CholecT50) and tool presence detection (+4.6pp of mAP in Cholec80). Moreover, even when using only half of the data, SurgFM outperforms state-of-the-art models in AutoLaparo and achieves state-of-the-art performance in Cholec80. Both Surg-3M and SurgFM have significant potential to accelerate progress towards developing autonomous robotic surgery systems. Our dataset, models, and code are publicly available at <https://github.com/visurg-ai/surg-3m>.

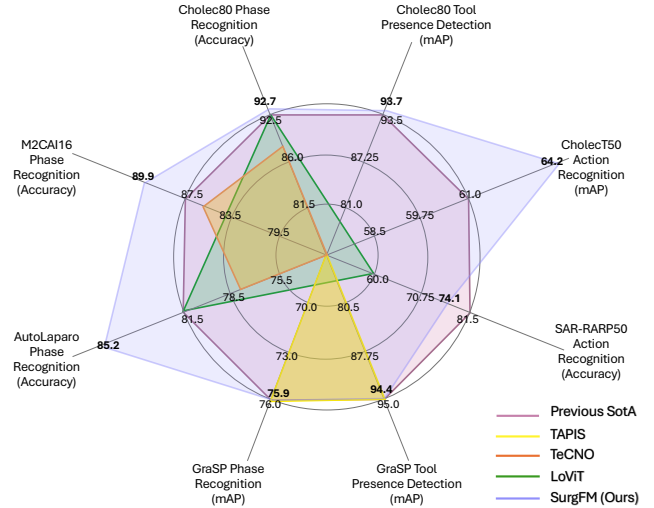


Figure 1. **Performance comparison between our foundation model, SurgFM, and the state-of-the-art (SotA) models.** Our evaluation focuses on three surgical downstream tasks and six datasets. SurgFM results are shown in bold. Axis labels are written in regular font. For a detailed breakdown of the results, see Tables 3, 4, and 5.

## 1. Introduction

Autonomous surgery has long been a promising area of research, with the potential to revolutionize the way surgical procedures are performed [25]. To achieve this goal, significant advancements in perception and computer vision are necessary, allowing robotic systems to accurately interpret and respond to the complexities of surgical environments [38]. However, training models for surgical perception is far from trivial due to the limited availability and high quality requirements of annotated data [39, 45, 59]. The complexities of medical data and stringent regulations governing patient privacy create significant hurdles for collecting and annotating relevant information [2, 19]. The cumulative effect of all these challenges has resulted in significantly limited computer vision datasets for surgical applications, with many containing fewer than 10K images [50]. These datasets, which may suffice for validation on specific

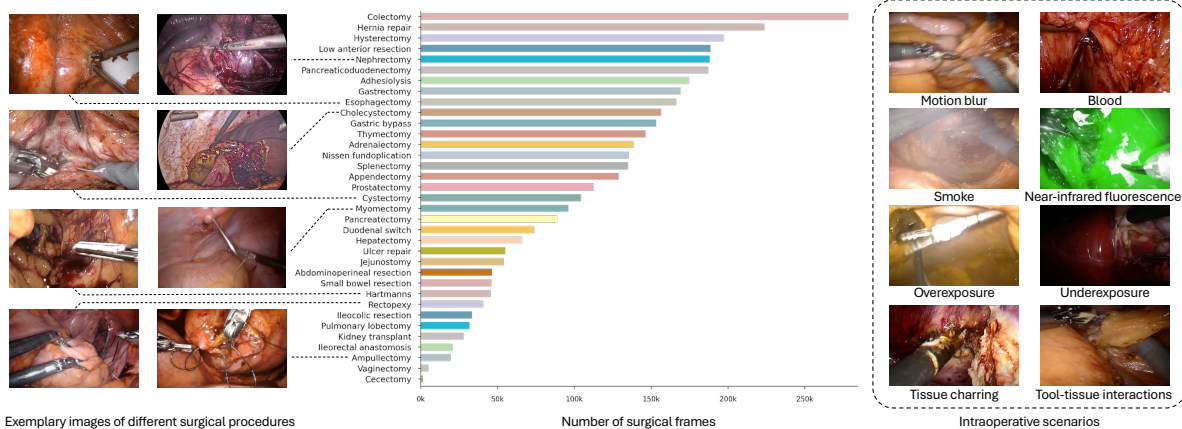


Figure 2. **Diversity and procedure prevalence in Surg-3M.** Representative samples from various procedures, demonstrating the diverse range of cases in our curated dataset (left, right). Distribution of surgical frames by procedure type (center).

computer vision tasks and surgical procedures, fall short in providing an adequate foundation for training models that can generalize effectively across diverse surgical settings and datasets.

Recent advances in self-supervised learning have opened up new research avenues, pretrained foundation models can significantly expedite progress, potentially reducing the need for annotated data by utilizing large-scale unlabeled datasets [49]. Despite this progress, ongoing data collection challenges persist, motivating the exploration of two key aspects: the sufficiency of publicly available surgical videos as a foundation for building a comprehensive dataset, and the potential of self-supervised models trained on this dataset to achieve state-of-the-art performance in surgical downstream tasks. By addressing these aspects, we aim to provide valuable insights into the feasibility and efficacy of using public domain data for training machine learning models in the field of surgical video analysis.

**Contributions.** We propose a novel data curation pipeline (Fig. 3) for collecting videos of selected surgical procedures, capturing exclusively surgical footage while discarding non-surgical content. Building upon this data curation pipeline, we present Surg-3M, a dataset for computer vision applications in surgery. Our Surg-3M dataset is large and diverse, containing 4K surgical videos and 3M images (Table 1). To the best of our knowledge, Surg-3M is the largest open-access surgical video dataset to date, 18× larger than the largest published surgical dataset [54]. To model the features of surgical video frames, we provide SurgFM, a pretrained model based on the ConvNeXt architecture [36] and DINO [8]. Additionally, we propose a novel augmented distillation method (Fig. 4) designed to enhance the local-to-global self-distillation mechanism described in [8]. SurgFM outperformed the current state-of-the-art models (Fig. 1) on Cholec80 [54], M2CAI16 [53],

Table 1. **Comparison of Surg-3M’s size to other existing public surgical datasets.** The number of frames is obtained by sampling videos at one frame per second.

Dataset	Year	# Procedure types	# Videos	# Frames
M2CAI16 [54]	2016	1	41	95K
Cholec80 [54]	2016	1	80	183K
CholecT50 [44]	2022	1	50	101K
AutoLaparo [57]	2022	1	21	83K
SAR-RARP50 [48]	2023	1	50	163K
GraSP [4]	2024	1	13	117K
<b>Surg-3M (ours)</b>	<b>2025</b>	<b>35</b>	<b>4194</b>	<b>3M</b>

[54], AutoLaparo [57], and CholecT50 [44]. Additionally, it helps to significantly reduce the annotation effort (Fig. 5). Building on our Surg-3M annotations, we introduce two new supervised learning applications: multi-label surgical procedure classification and surgery type classification. Leveraging our image foundation model, SurgFM, we propose SurgFM-Vid, a video classifier that achieves top performance on these new tasks, serving as a baseline for future research.

## 2. Related Work

**Surgical datasets.** Previous works have released open-access datasets aimed at addressing specific surgical downstream tasks and procedures (Table 1). Despite their valuable contributions, these open-access datasets suffer from a narrow scope of surgical procedures and limited dataset sizes. Besides these open-access datasets, there are several private surgical datasets, including SVL [63], with 1.4K videos, and SAGES CVS [47], with 1K videos. However, the restricted accessibility of these datasets constrains their utility and hinders their potential for more widespread use. To overcome these limitations, our work introduces Surg-3M. Compared with Cholec80 [54], the largest open-access

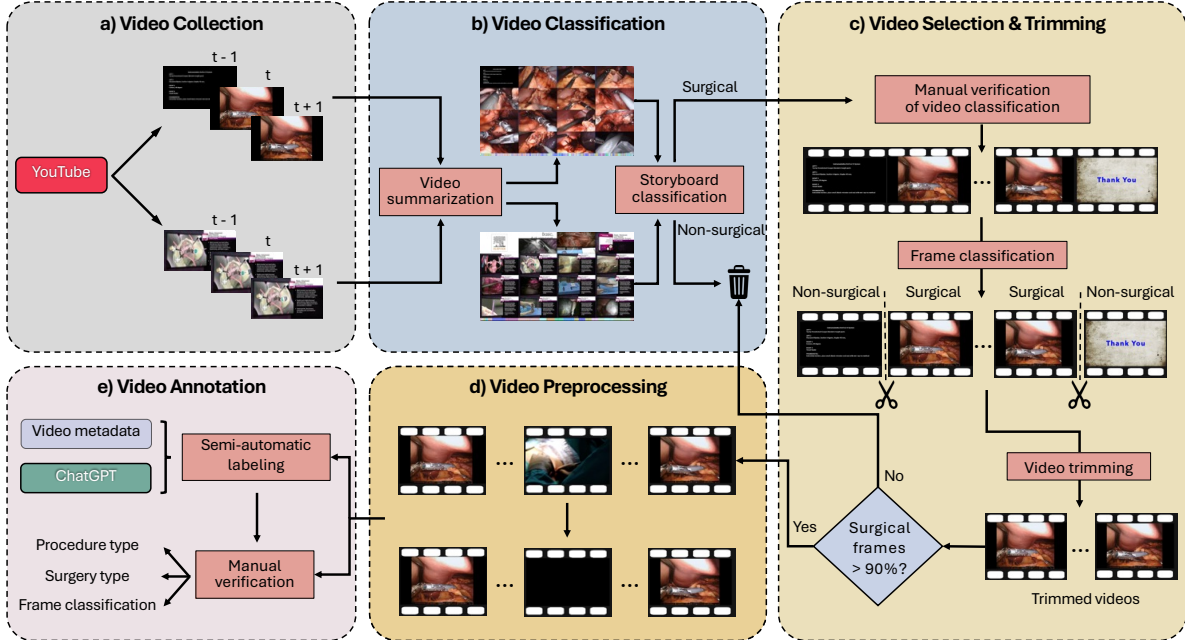


Figure 3. **Data curation pipeline.** (a) Surgical videos are collected from YouTube. (b) The videos are summarized as storyboards (trivial to annotate and classify). We train a storyboard classifier to identify videos with rich surgical content, and manually verify the selected videos. (c) During the video selection and trimming phase, a trained frame classifier categorizes each frame as either *surgical* or *non-surgical*, allowing us to trim non-surgical frame segments at the beginning and end of each video. We further filter videos by requiring at least 90% of their frames to be surgical frames. (d) In the video preprocessing stage, we obliterate non-surgical frames. (e) During the video annotation phase, we utilize the video title as a primary cue to determine the procedure and surgery type. In cases where the video titles do not explicitly include any of our procedure name keywords (Fig. 2), we employ ChatGPT to match the titles with surgical procedure types. The set of final videos, and their corresponding labels, are manually quality controlled.

surgical dataset, Surg-3M provides  $18\times$  more surgical images and  $35\times$  the surgical procedure types.

**Self-supervised learning.** Self-supervised learning (SSL) has gained significant attention due to its ability to reduce reliance on large-scale annotated datasets, a benefit that is particularly relevant for surgical applications. Recently, Ramesh et al. [49] investigated the effectiveness of different SSL approaches for surgical applications, including MoCov2 [11], SwAV [7], SimCLR [10], and DINO [8]. Their experiments showed that DINO consistently outperformed other SSL methods on both surgical phase recognition and surgical tool presence detection tasks, highlighting its potential in surgical applications.

As part of a broader effort to advance self-supervised surgical models, Hirsch et al. [24] built a private surgical dataset and trained Masked Siamese Networks (MSN) [3] on this dataset, achieving near-state-of-the-art results. While the research presented in this study shows promising results, its broader applicability and reproducibility are somewhat constrained by the lack of public availability of the underlying dataset, as well as a relatively narrow evaluation scope that only considers performance on two specific task-dataset pairs: surgical phase recog-

nition on Cholec80 [54], and polyp characterization on PolypSet [32]. Similarly, in Endo-FM [58], the authors proposed to train a student-teacher foundation model on a composite dataset that combined private and public data sources. Although showing encouraging results, the approach is also of limited accessibility. More recently, Batic et al. [5] created a dataset of 70K images merging nine public datasets. They trained a model based on masked autoencoders (MAE) [23], but showed limited performance, likely due to their reduced dataset size.

### 3. Proposed Surg-3M Dataset

To develop a robust surgical foundation model, it is essential to create a comprehensive, large-scale dataset of diverse surgical images that covers the whole spectrum of minimally invasive surgical procedures executed within the operating room. To fulfill this need we propose Surg-3M, a dataset that contains 4K videos and 3M images corresponding to 35 different surgical procedures, including videos from robotic-assisted surgeries and non-robotic traditional laparoscopies (more details on these surgical techniques are provided in Sec. A of the supplementary material).

**Ground truth and proposed new tasks.** Each of the

Table 2. **Ablation studies providing justification for SurgFM design choices.** The predictions are computed on a frame-by-frame basis for all tasks, no temporal information is used. The S3M superscript indicates that the model was fine-tuned on Surg-3M. The SurgFM<sup>S3M</sup> model is DINO-ConvNeXt-L<sup>S3M</sup> plus augmented distillation, presented in Sec. 4. Standard deviation is estimated using 5-fold cross-validation.

Method	Phase recognition (Cholec80)		Tool detection (Cholec80)		Action recognition (CholecT50)	
	Accuracy (%)	F1-score (%)	mAP (%)	F1-score (%)	mAP (%)	F1-score (%)
DINO (frozen) [8]	69.8 ± 1.5	62.5 ± 1.5	67.8 ± 3.1	59.3 ± 4.0	36.1 ± 1.4	28.9 ± 2.7
DINOv2 (frozen) [46]	67.0 ± 1.7	60.3 ± 1.8	56.1 ± 3.4	41.2 ± 2.6	27.2 ± 2.2	17.2 ± 0.8
MAE (frozen) [23]	55.2 ± 1.4	49.6 ± 1.2	40.4 ± 1.4	22.9 ± 0.9	20.7 ± 1.3	13.4 ± 1.3
DINO-ConvNeXt-L <sup>S3M</sup>	84.0 ± 1.8	76.7 ± 2.7	92.9 ± 0.7	88.4 ± 1.2	58.8 ± 1.3	52.0 ± 1.8
DINO-ViT-L <sup>S3M</sup>	83.7 ± 1.8	76.0 ± 2.6	91.5 ± 0.7	86.1 ± 0.8	57.5 ± 1.6	52.4 ± 2.4
SurgFM <sup>S3M</sup> (ours)	<b>84.3 ± 0.5</b>	<b>76.7 ± 1.4</b>	<b>94.0 ± 0.6</b>	<b>89.6 ± 0.9</b>	<b>59.5 ± 1.6</b>	<b>53.4 ± 1.1</b>

4K surgical videos is annotated for two tasks: 1) multi-label procedure type classification, where the objective is to identify the procedure[s] performed in an intervention’s video from among 35 possible options (Fig. 2); and 2) binary surgery type classification, where the goal is to indicate whether a surgery is conducted robotically or non-robotically. The rationale for these annotations is two-fold. Firstly, it allows us to validate the comprehensiveness of our dataset by ensuring that it encompasses a broad spectrum of surgical procedures. Secondly, it facilitates the development of new methods that use this information as a key input (e.g., our SurgFM foundation model, video classification/retrieval, video similarity measurement, procedure-specific estimation of surgical remaining time).

Scenes in surgical videos unfold at a relatively slow pace, as surgeons must ensure patient safety. Consequently, our 3M image dataset was compiled by sampling our dataset of 4194 curated videos at 1 fps, which is standard practice in the field of surgical computer vision [44, 48, 53, 54, 57]. In the following sections we detail how we collected, curated, and annotated these videos. An overview of the curation pipeline is shown in Fig. 3.

### 3.1. Dataset Curation

**Video collection.** Inspired by works in other fields [1, 9, 15, 40, 61], we collected our videos from YouTube. For each of the 35 procedures in Fig. 2, we searched for videos of their robotic and non-robotic variants using the strings “robotic <procedure type>” and “laparoscopic <procedure type>”, respectively. We run the video collection process until we had 500 different videos collected for each procedure leading to a total of ≈18K raw videos.

**Video classification.** The raw videos collected based on search keywords contained a diverse range of content, including patient testimonials and conference presentations. To avoid including non-surgical videos in our dataset, we classified the videos as surgical and non-surgical (Fig. 3b). This pipeline consisted of three stages. First, a dataset of 2160 surgical and 1910 non-surgical video storyboards (Fig. 3b) was annotated. Second, a binary video storyboard classifier was trained on this dataset and run over all the raw

videos. Finally, manual verification was performed on the videos classified as surgical.

**Video selection and trimming.** A video classified as surgical may still contain non-surgical frames (e.g., presentation slides). Therefore, we trained a surgical frame classifier and used it to 1) trim the non-surgical content present at the beginning and end of videos, and 2) discard videos containing more than 10% of the frames estimated as non-surgical after trimming (Fig. 3c).

**Video preprocessing.** We use our previously trained frame classifier to detect and obliterate those frames that are estimated to be non-surgical within the trimmed videos. After this process, we manually quality control the videos to verify that their frames are surgical.

**Video annotation.** We cross-reference the video titles with the predefined list of procedures. When exact title matches are not found, we leverage the capabilities of the ChatGPTv4 API to perform a more nuanced analysis, incorporating a customized prompt as specified in Sec. B of the supplementary material. All annotations are manually reviewed and validated to ensure the accuracy of the labels assigned.

## 4. Proposed SurgFM Foundation Model

In this section, we describe how we build SurgFM, our foundation model trained on Surg-3M, and motivate its design choices. This section includes two ablation studies to identify the optimal self-distillation configuration and the most suitable backbone architecture for surgical videos; a description of our image preprocessing pipeline, and our proposed augmented distillation mechanism with its corresponding ablation study. The results of the ablation experiments are presented in Table 2.

**Self-supervised methods.** We examine the impact of the different self-supervision mechanisms (Table 2). We evaluate DINO [8], DINOv2 [46], and MAE [23]. For these experiments, we trained the models in their standard configurations, a ViT-B backbone [14] pretrained on ImageNet-1k [13] with frozen weights and a linear classification head. Stemming from these results, which align with those in the literature [49], DINO consistently outperforms DINOv2

and MAE on all downstream tasks, with surgical tool detection and action recognition showing a large margin. Therefore, we adopt DINO’s self-distillation [8] as our pretext task for self-supervision.

**Backbone models.** As noted in [56], ViTs [14] face challenges to capture fine details, which is essential to solving tasks such as tool presence detection and surgical action recognition. Given this, we opted to evaluate the performance of ViT-L [14] against a modern convolutional architecture, ConvNeXt-L [36]. Both were pretrained on Surg-3M and fine-tuned on Cholec80 [54] and CholecT50 [42], for surgical phase recognition, tool presence detection, and surgical action recognition. The results are shown in Table 2. ConvNeXt-L outperformed ViT-L, suggesting that convolutional networks are indeed better equipped to capture those fine image details that are relevant to solve surgical tasks. Therefore, we use ConvNeXt-L as the backbone of our SurgFM model.

**Image preprocessing pipeline.** Surgical videos often exhibit superimposed manufacturer-specific user interface (UI) information generated by the software of the surgical stack. While certain researchers might derive value from analyzing these UI elements (e.g., some interfaces provide contextual information regarding the surgical instruments utilized in the video), a foundational model for surgery should prioritize learning correlations between tissue appearance and tool-tissue interactions. This focus is essential to avoid acquiring spurious correlations with manufacturer-specific UI elements. Therefore, we manually annotated 2719 surgical frames with 4584 non-surgical bounding-box instances and trained a YOLOv8 Nano model [31] to detect and crop out UI content (see Fig. S2 in supplementary material).

**Proposed augmented distillation method.** Inspired by DINO [8], we train a student network  $f_{\theta_s}$  to solve for the mapping  $\sigma(f_{\theta_t}(\mathbf{x})) = \sigma(f_{\theta_s}(\mathbf{x}))$  where  $\mathbf{x} \in \mathbb{R}^{H \times W \times 3}$  is an input image,  $\sigma$  is the softmax function,  $f_{\theta_t}(\mathbf{x}) \in \mathbb{R}^C$  is a target vector of dimension  $C = 2^{16}$  estimated from a teacher network  $f_{\theta_t}$ , and  $\theta_s$  and  $\theta_t$  are the parameters of the student and teacher models, respectively. We use the outputs of both networks to build two categorical distributions,  $P_s(z|\sigma(f_{\theta_s}(\mathbf{x}))) = \sigma_z(f_{\theta_s}(\mathbf{x}))$  and  $P_t(z|\sigma(f_{\theta_t}(\mathbf{x}))) = \sigma_z(f_{\theta_t}(\mathbf{x}))$ , where  $\sigma_z$  denotes the  $z^{\text{th}}$  element of the softmax output, and  $z \in \{1, \dots, C\}$ . In training, we minimize the negative log-likelihood of  $P_s(z|\sigma(f_{\theta_s}(\mathbf{x})))$  following

$$\min_{\theta_s} \sum_{i=1}^I \sum_{\substack{\mathbf{u} \in U_i \\ \mathbf{v} \in V_i \cup W_i \\ \mathbf{u} \neq \mathbf{v}}} [d(\mathbf{u}, \mathbf{v}) - n(\mathbf{u}, \mathbf{v})] \quad (1)$$

where  $d(\mathbf{u}, \mathbf{v}) = \log \sum_{k'=0}^{C-1} \exp(\sigma_{k'}(f_{\theta_s}(\mathbf{v})))$ ,  $n(\mathbf{u}, \mathbf{v}) = \sigma_{\arg \max_z P_t(z|\sigma(f_{\theta_t}(\mathbf{u})))}(f_{\theta_s}(\mathbf{v}))$ ,  $I$  is the number of images in the dataset,  $U_i$  contains two global augmentations

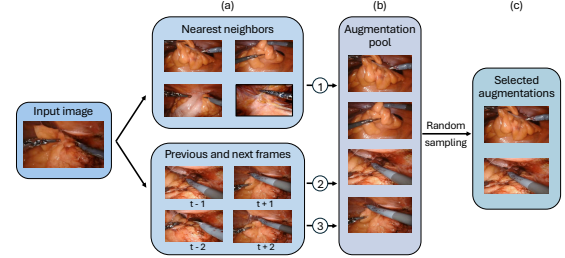


Figure 4. **Proposed augmented distillation method.** To encourage invariance in SurgFM to minor surgical motion and subtle appearance changes across surgeries, we introduce  $W_i$  (Eq. 1). The key component of  $W_i$  is a pair of images (c) that are randomly selected from an augmentation pool (b). To populate the augmentation pool, which has capacity for four images, we first retrieve the nearest neighbors<sup>(1)</sup> of the input image from other videos of the same procedure type, but only include them in the pool if the cosine distance to the input image is smaller than  $3 \times$  the distance between the input image and its preceding frame in the video that it was extracted from. When not enough suitable neighbors are found, we supplement the pool with adjacent video frames<sup>(2)(3)</sup>.

of  $\mathbf{x}_i$ , and  $V_i$  contains two global augmentations and four augmented crops of  $\mathbf{x}_i$ . A foundation model for surgery should learn invariance to 1) minor movements of instruments and tissues observed between adjacent video frames, and 2) minimal appearance changes across patients undergoing the same surgical procedure (e.g., organ color variations). Diverging from DINO [8], and relying on the annotations available in Surg-3M, we introduce  $W_i$  to provide a supervisory signal that encourages the model to learn these invariances.  $W_i$  contains two images, and four augmented crops of these two images. The procedure for selecting these two images is depicted in Fig. 4. We use the  $k$ -nearest neighbors (in embedded space) of the input image from other videos of the same procedure type to learn invariance to appearance changes across patients, and the prior and subsequent video frames of the input image to learn invariance to the motion occurring between consecutive frames.

We evaluate the performance of models trained with and without our augmented distillation (see Table 2) on surgical phase recognition (Cholec80), tool presence detection (Cholec80), and surgical action recognition (CholecT50). With augmented distillation, F1-score improved by  $> 1pp$  in both tool detection and action recognition tasks.

Following these ablation results, we incorporated augmented distillation in our final SurgFM model.

**Proposed video classification model.** Considering that each surgical procedure is localized to a specific region of the body, we posit that a characteristic scene can be associated with each procedure. Based on this assumption, and inspired by active learning [21], we propose SurgFM-Vid, a video classification method that employs SurgFM embed-

Table 3. **Performance evaluation on surgical phase recognition.** The models are tested on four datasets: Cholec80 [54], AutoLaparo [57], M2CAI16 [54], and GraSP [4]. The evaluation metrics used in this table are described in Sec. 5.1. The evaluation protocol and the meanings of G, S, and F in the *type* column are described in Sec. 5.2. The † superscript next to Cholec80 and M2CAI16 indicates the use of the standard 10-second relaxed boundary in phase transitions [54]. The superscript \* denotes that the SurgFM backbone is frozen. Temporal information is used in these experiments. The subscript ± denotes methods that utilize both past and future frames [4, 17, 55], otherwise only past frames are used. **Best viewed online.**

Method	Type	Cholec80†					AutoLaparo				M2CAI16†				GraSP
		Accuracy (%)	Precision (%)	Recall (%)	Jaccard (%)	F1-score (%)	Accuracy (%)	Precision (%)	Recall (%)	Jaccard (%)	Accuracy (%)	Precision (%)	Recall (%)	Jaccard (%)	mAP (%)
ConvNcKt-L [36]	G	91.4 ± 6.7	92.3 ± 3.8	90.5 ± 7.7	82.1 ± 7.1	88.6 ± 6.8	82.3 ± 9.7	78.3 ± 21.9	69.9 ± 31.9	60.5 ± 27.2	88.3 ± 10.0	89.4 ± 4.7	89.5 ± 3.3	78.4 ± 6.2	73.4
EndoNet [54]		81.7 ± 4.2	73.7 ± 16.1	79.6 ± 7.9	-	76.5	-	-	-	-	-	-	-	-	-
MTRCNet-CL [27]		89.2 ± 7.6	86.9 ± 4.3	88.0 ± 6.9	-	87.4	-	-	-	-	-	-	-	-	-
PhaseNet [52]		78.8 ± 4.7	71.3 ± 15.6	76.6 ± 16.6	-	73.8	-	-	-	79.5 ± 12.1	-	-	64.1 ± 10.3	-	
SV-RCNet [26]		85.3 ± 7.3	80.7 ± 7.0	83.5 ± 7.5	-	82.1	75.6	64.0	59.7	47.2	81.7 ± 8.1	81.0 ± 8.3	81.6 ± 7.2	65.4 ± 8.9	
OHFM [62]		87.3 ± 5.7	-	-	67.0 ± 13.3	-	-	-	-	-	85.2 ± 7.5	-	-	68.8 ± 10.5	
TeCNO [12]		88.6 ± 7.8	86.5 ± 7.0	87.6 ± 6.7	75.1 ± 6.9	-	77.3	66.9	64.6	50.7	86.1 ± 10.0	85.7 ± 7.7	88.9 ± 4.5	74.4 ± 7.2	
TMRNet [29]	S	90.1 ± 7.6	90.3 ± 3.3	89.5 ± 5.0	79.1 ± 5.7	-	78.2	66.0	61.5	49.6	-	-	-	-	
AVT [20]		-	-	-	-	-	77.8 ± 9.4	68.0	62.2	50.7	-	-	-	-	
Trans-SVNet [30]		90.3 ± 7.1	90.7 ± 5.0	88.8 ± 7.4	79.3 ± 6.6	-	78.3	64.2	62.1	50.7	87.2 ± 9.3	88.0 ± 6.7	87.5 ± 5.5	74.7 ± 7.7	
LoVit [35]		92.4 ± 6.3	89.9 ± 6.1	90.6 ± 4.4	81.2 ± 9.1	-	81.4 ± 7.6	85.1	65.9	55.9	-	-	-	-	
SlowFast± [17]		-	-	-	-	-	-	-	-	-	-	-	-	-	
TAPIR± [55]		-	-	-	-	-	-	-	-	-	-	-	-	70.1	
TAPIS± [4]		-	-	-	-	-	-	-	-	-	-	-	-	74.6	
Ramesh et al. [49]		-	-	-	-	81.6	-	-	-	-	-	-	-	76.1	
SSL4EVA [24]		-	-	-	-	86.9	-	-	-	-	-	-	-	-	
EndoViT [5]	F	89.4	-	-	-	-	-	-	-	-	-	-	-	-	
SurgFM* (ours)		87.0 ± 10.3	87.3 ± 7.5	87.7 ± 4.3	75.7 ± 9.2	83.1 ± 11.0	81.7 ± 10.9	<b>86.3 ± 8.9</b>	69.8 ± 30.9	60.2 ± 26.1	82.6 ± 10.7	85.5 ± 9.9	87.3 ± 5.9	73.2 ± 9.4	66.8
SurgFM (ours)		<b>92.7 ± 8.3</b>	<b>93.0 ± 4.5</b>	<b>93.1 ± 4.7</b>	<b>85.1 ± 7.9</b>	<b>90.6 ± 6.7</b>	<b>85.2 ± 9.9</b>	82.9 ± 17.3	<b>73.2 ± 32.0</b>	<b>64.8 ± 27.3</b>	<b>89.9 ± 7.1</b>	<b>89.6 ± 6.5</b>	<b>89.9 ± 6.9</b>	<b>79.4 ± 9.9</b>	75.9

dings for video classification by aggregating them following

$$\mathbf{v}_e = \sum_{j=0}^{J-1} \omega_j \phi_j \quad (2)$$

where  $\mathbf{v}_e$  is a video embedding,  $J$  is the number of frames in the video,  $\omega_j = \frac{t(\phi_j)}{\epsilon + \sum_{m=0}^{J-1} t(\phi_m)}$ ,  $\phi_j$  is the embedding of frame  $j$ ,  $t(\phi) = \left( \frac{1}{K} \sum_{\eta \in K-NN(\phi)} d(\phi, \eta) \right)^{-1}$  is the typicality [21] of a frame,  $K - NN(\phi)$  with  $K = 20$  are the nearest neighbors of  $\phi$ ,  $d$  is the cosine distance, and  $\epsilon = 10^{-8}$ . Then, each  $\mathbf{v}_e$  is classified with a single-layer MLP.

## 5. Evaluation

### 5.1. Downstream Tasks, Datasets and Metrics

We evaluate SurgFM on three surgical downstream tasks: surgical phase recognition [4, 53, 54, 57], surgical tool presence detection [4, 54], and surgical action recognition [4, 48]. To do so, we use the most widely adopted datasets, data splits, and evaluation metrics.

**Surgical phase recognition.** We use M2CAI16 [54], Cholec80 [54], AutoLaparo [57], and GraSP [4]. For this task, we report accuracy, precision, recall, Jaccard, F1-score, and mean Average Precision (mAP). The accuracy for a video is computed by dividing the number of frames whose class has been correctly predicted by the total number of frames. The overall accuracy for a dataset is defined as the mean accuracy value over all videos, henceforth referred to as *video-level* accuracy [27–29, 35]. Precision, recall, and Jaccard are computed differently than accuracy [27–29, 35]. These three *phase-level* metrics are computed for each class and video, then averaged: first within videos, and secondly across classes. The F1-score, computed for Cholec80, is also computed for each class and

video, but averaged first over classes and then over videos, and referred to as *video-level* F1-score [24, 49]. For GraSP, the *frame-level* mAP was calculated by averaging the mAP scores across all frames in the test set [4].

**Surgical tool presence detection.** Cholec80 and GraSP are utilized in the surgical phase recognition task. We report mAP across all frames in the testing dataset [4, 49].

**Surgical action recognition.** For this task we use CholecT50 [44] and SAR-RARP50 [48]. For CholecT50, we report the *video-level* mAP, which is computed by first calculating the average mAP for each class across all videos and then taking the overall mean of these class averages [44]. For SAR-RARP50 [48], we report *video-level* accuracy and *video-level* F1 @ 10 [48].

### 5.2. Downstream Task Evaluation Protocols

To capture temporal correlations in the **surgical phase recognition** downstream task, we couple our SurgFM backbone with a TCN head [12]. This TCN head takes both current and previous frames into account, but excludes future frames. For a fair comparison with previous methods [12, 26, 27, 30, 35, 54], we run our evaluation in Cholec80 and M2CAI16 with the standard 10-second relaxed boundary between some of the surgical phases [54]. Also to be able to compare with previous literature [4, 35, 57], we do not use a relaxed boundary for AutoLaparo and GraSP.

For **surgical tool presence detection**, we use a linear head for all datasets.

For **surgical action recognition** we use a different head for each dataset. To evaluate on CholecT50, we utilize a linear head. The predictions are done per-frame, no temporal information is used, as in the approaches that we benchmark against [43, 44]. For SAR-RARP50, we evaluate our model in two different modes: *online*, where only previous frames are available (TCN head [12]), and *offline* ( $\pm$  subscript in Table 5), which incorporates information from both previ-

Table 4. **Performance evaluation on surgical tool presence detection.** We evaluate the performance on two datasets: Cholec80 [54], and GraSP [4]. The metrics are computed as described in Sec. 5.1. The evaluation protocol and the meanings of G, S, and F in the *type* column are described in Sec. 5.2. The superscript \* denotes that the backbone is frozen during fine-tuning.

Method	Type	Cholec80	GraSP
		mAP (%)	mAP (%)
ConvNeXt-L* [36]	G	69.3	68.1
ConvNeXt-L [36]		93.3	89.5
EndoNet [54]	S	81.0	-
MTRCNet-CL [27]		89.1	-
Rendezvous [44]		-	80.4
TAPIS [4]		-	<b>95.1</b>
Ramesh et al. [49]		93.6	-
SurgFM* (ours)	F	76.1	76.4
SurgFM (ours)		<b>93.7</b>	94.4

ous and future frames (MS-TCN head [33]), to ensure a fair comparison with all competing methods in [48].

In our evaluation, we compare three types of models: generalist (G), pretrained on ImageNet and fine-tuned for each downstream task; specialist (S), designed for specific downstream tasks; and foundational (F), pretrained in a self-supervised manner and fine-tuned on each downstream task.

## 6. Results and Discussion

### 6.1. Ablation Studies

**SurgFM design choices.** We performed incremental ablation studies that test the choice of backbone (ViT vs ConvNeXt), self-supervision method (DINO vs DINOv2 vs MAE), and our proposed augmented distillation (Sec. 4). The results are shown in Table 2. DINO outperformed DINOv2 and MAE in all the downstream tasks and metrics evaluated, with improvements  $>8$  percentage points (pp) in mAP in both tool detection and action recognition. ConvNeXt-L achieved comparable results to ViT-L in phase recognition, and improved  $>2$ pp (F1-score) in surgical tool detection and  $>1$ pp (mAP) in surgical action recognition. Our proposed augmentation achieved comparable results in phase recognition, and improved  $>1$ pp (mAP) in tool detection and  $>1$ pp (F1-score) in action recognition.

**Pretrained weights.** We compare the effects of employing pretrained weights from ImageNet in the ConvNeXt-L backbone with those of using Surg-3M. As shown in Tables 3, 4, and 5, SurgFM (which also has a ConvNeXt-L backbone, but is pretrained on Surg-3M) outperformed the ConvNeXt-L backbone pretrained on ImageNet in all downstream tasks and datasets. This finding suggests that SurgFM serves as a superior starting point for surgery-specific downstream task fine-tuning compared to models pretrained on general-purpose datasets like ImageNet. This is clearly shown in the surgical tool presence detection experiments (Table 4) on the GraSP dataset, where SurgFM outperformed a ConvNeXt-L pretrained on ImageNet by

Table 5. **Performance evaluation on surgical action recognition.** Two datasets are used: CholecT50 [42] and SAR-RARP50 [48]. The metrics are computed as described in Sec. 5.1. The evaluation protocol and the meanings of G, S, and F are explained in Sec. 5.2. The superscript \* denotes that the SurgFM backbone is frozen during fine-tuning. The subscript  $\pm$  indicates that both past and future frames are used [48].

Method	Type	CholecT50	SAR-RARP50	
		mAP (%)	Accuracy (%)	FI@10 (%)
ConvNeXt-L $\pm$ [36]	G	62.9 $\pm$ 2.3	71.9	70.4
Tripnet [43]	S	58.8 $\pm$ 3.1	-	-
Rendezvous [44]		60.4 $\pm$ 2.8	-	-
Attention Tripnet [44]		61.1 $\pm$ 2.0	-	-
SummerLab-AI $\pm$ [48]		-	<b>81.5</b>	<b>84.1</b>
Uniandes $\pm$ [48]		-	78.6	82.3
MS-TCN $\pm$ [16, 48]		-	69.0	70.7
LoViT $\pm$ [35, 48]		-	59.8	43.0
SurgFM (ours)		<b>64.2 <math>\pm</math> 1.7</b>	70.2	68.4
SurgFM* (ours)	F	63.7 $\pm$ 1.7	72.4	74.3
SurgFM $\pm$ (ours)		<b>64.2 <math>\pm</math> 1.7</b>	74.1	74.3

more than 4pp in mAP.

### 6.2. Comparison with Sota

The performance of our SurgFM compared to the state of the art in each downstream task and dataset is shown in Fig. 1 and Tables 3, 4, and 5.

**Surgical phase recognition.** As shown in Table 3, SurgFM outperformed all specialist [12, 20, 26, 27, 29, 30, 35, 52, 54, 62] and foundation [5, 24, 49] models in Cholec80 ( $>3$ pp Jacc.), AutoLaparo ( $>8$ pp Jacc.), and M2CAI16 ( $>4$ pp Jacc.). These results demonstrate that SurgFM is able to effectively extract features that are useful for different surgical procedures, capitalizing on the diversity of surgery types present in the Surg-3M dataset.

In GraSP, SurgFM demonstrated performance comparable (with an mAP difference of  $<1$ pp) to that of the methods presented in [4, 17, 55]. However, these competing methods [4, 17, 55] utilize both past and future frames (offline), whereas our SurgFM is restricted to observing only the current and preceding frames, reflecting its real-time operational focus, and its broader range of application [35]. Despite being constrained by its limited temporal perspective, SurgFM achieves comparable performance with these more information-rich approaches.

**Surgical tool presence detection.** As shown in Table 4, SurgFM outperformed all specialist [27, 44, 54] and foundation [49] models in Cholec80, and achieved a comparable performance to [4, 44] in GraSP.

**Surgical action recognition.** As shown in Table 5, SurgFM outperformed all specialist model [43, 44] in CholecT50 ( $>3$ pp mAP), and achieved a competitive performance to [48] in SAR-RARP50 ( $<7$ pp difference in accuracy).

**Frozen SurgFM model.** As shown in Tables 3, 4, and 5, the frozen version of SurgFM, denoted SurgFM\*, is indeed a foundation model. It works on all datasets and tasks with-

Table 6. **Leaderboard for the proposed tasks on Surg-3M.** Multi-label (35 classes) video classification of procedure types and binary classification of surgery types.

Method	Procedure type		Surgery type	
	mAP (%)	F1 (%)	Accuracy (%)	F1 (%)
SlowFast [17]	22.0	23.9	88.5	87.5
TimeSformer [6]	42.1	37.5	93.2	92.7
MViTv2 [34]	49.5	41.8	95.8	94.6
Video Swin Transformer [37]	51.4	47.9	98.8	98.7
SurgFM-Vid (ours)	<b>57.8</b>	<b>49.3</b>	<b>98.9</b>	<b>98.9</b>

out retraining. In Cholec80, SurgFM\* outperforms specialist SotA architectures such as EndoNet, PhaseNet, and SV-RCNet, OHFM, TeCNO. In AutoLaparo, SurgFM\* outperforms all the six specialist models we compared it with. In M2CAI16, SurgFM\* outperforms two specialist SotA models, PhaseNet and SV-RCNet. In SAR-RARP50, SurgFM\* outperforms MS-TCN and LoViT.

**Data scaling.** We investigated the extent to which annotation effort can be alleviated by leveraging our pre-trained SurgFM model. To do so, we fine-tuned it on downstream tasks with 10%, 50%, and 100% of the annotated data (Fig. 5). With 50% of the data, the performance decreased a maximum of 4.4pp across all datasets and tasks except GraSP, which has a total of four videos for training at 100%, and where performance dropped by 9.6pp. The closest result was achieved in phase recognition (Cholec80), with SurgFM achieving an accuracy of 92.3% on 50% of the data, only 0.1pp below prior SotA with 100% of the data [35]. Also at 50%, our SurgFM outperformed prior SotA [35] in AutoLaparo at 100%. These results suggest that the features learned by SurgFM from Surg-3M are highly informative. Comparing our results with other foundation models reported in the literature, SurgFM achieved >6pp (F1-score) than Ramesh et al. [49] in phase recognition (Cholec80), despite using only 10% of the data compared to their 12.5%. Furthermore, SurgFM also outperformed Ramesh et al. by >6pp (mAP) on tool presence detection (Cholec80) at 10%.

### 6.3. Leaderboard

To establish a baseline for the novel tasks presented in Sec. 3, we conducted an evaluation of SotA approaches on Surg-3M (Table 6), which serves as a benchmark for future research endeavors. By leveraging the robust representations extracted from SurgFM, our video classification model, SurgFM-Vid (Sec. 4), demonstrated significant improvements (>6 mAP) over all the leading video classification models tested on the multi-label procedure type classification task. On the binary surgery type classification task, our approach achieved comparable accuracy to the top performer, the Video Swin Transformer [37]. The incorporation of frame-level features extracted by SurgFM, in conjunction with the strategic application of prior knowledge

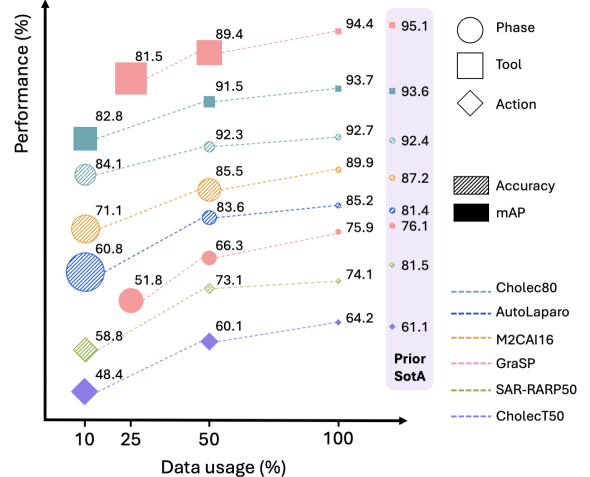


Figure 5. **Data scaling.** Results of SurgFM when fine-tuned on the downstream tasks with different percentages of annotated training samples. The radius of the circles, computed following  $2 \log(\sigma + 1)$ , represents the standard deviation ( $\sigma$ ) of each metric estimated over five cross-validation folds. Prior SotA is computed using 100% of the available data. **Best viewed online.**

through weighted feature embeddings informed by frame typicality, leads to substantial performance gains, underscoring the value of SurgFM as a critical component in surgical video analysis tasks. Despite these improvements, our results also highlight the challenges associated with surgical procedure classification, underscoring the need for continued innovation in this area.

## 7. Conclusion

Building on a large corpus of publicly available surgical videos, this work has two main contributions: we have created a large-scale and diverse surgical video dataset, Surg-3M, and a foundation model, SurgFM. Our SurgFM outperformed specialist architectures on four datasets and three downstream tasks, demonstrating its potential as a valuable tool for computer vision research in surgery. Furthermore, our experimental results show that SurgFM can maintain its performance with significantly reduced data annotation needs (50% or even 10% for some tasks), highlighting the efficiency of our approach. This work showcases the value of Surg-3M and SurgFM as a foundation for future research in surgical computer vision. To further improve these contributions, we plan to address key limitations of our current approach, including adapting SurgFM to pixel-wise tasks and enhancing the self-distillation approach to better adapt to surgical data. Ultimately, this work highlights the importance of publicly available surgical videos in developing more effective models for computer vision research in surgery, and we believe that Surg-3M and SurgFM will serve as catalysts for future advancements in this field.

# Surg-3M: A Dataset and Foundation Model for Perception in Surgical Settings

## Supplementary Material

### A. Surgical Background

In contrast to traditional open surgery (not the target of our work), which entails extensive tissue disruption via large incisions and relies on direct visual inspection by the surgeon (i.e., no cameras are used), modern surgical practices predominantly employ minimally invasive techniques (the target of our work). These techniques involve the insertion of slender instruments, including one that is a camera, into the patient’s body through small incisions.

To control the instruments from outside the patient’s body, there are two variants: robotic-assisted surgery (called “robotic” in our manuscript) and non-robotic laparoscopy (called “non-robotic” in our manuscript). Robotic-assisted surgery involves a surgeon sitting on a console and controlling (with joysticks) several robotic arms that hold and steer the instruments inside the patient. In contrast, non-robotic (also known as traditional or conventional) laparoscopy requires the surgeon to directly hold and steer the laparoscopic hand-held instruments (i.e., no robotic arms involved).

### B. Details of Data Curation

This section provides details of the implementation of our data curation pipeline.

#### B.1. Video Classification

**Video summarization.** To improve the efficiency of annotating surgical and non-surgical videos, we obtained  $4 \times 4$ -image video storyboards (i.e. a single image containing a collage of key video frames) for all the collected videos using the method described in [18]. Storyboards enabled us to quickly determine whether a video contained substantial surgical footage, thereby avoiding the need for complex analysis on the entire sequence.

**Video storyboard classification.** We manually annotated a dataset comprising 2160 surgical and 1910 non-surgical storyboards. The annotation criterion adopted for labeling a storyboard as *surgical* was that at least 50% of the key frames contained shots from a surgical camera; specifically, open surgery videos were categorized as non-surgical. To classify the rest of the collected videos, we trained a ResNet18 [22]. To ensure the accuracy of the inference results, we manually reviewed all the videos classified as surgical.

**Performance of video storyboard classification models.** We trained five video storyboard classification models (different data splits) to categorize the videos as either surgical or non-surgical. Each fold was split into training,

Table S1. Performance of the video storyboard classification models across five folds.

Fold	F <sub>1</sub> -score (%)	Accuracy (%)	Precision (%)	Recall (%)
Fold 0	94.42	94.50	95.88	93.00
Fold 1	93.60	93.50	92.23	95.00
Fold 2	93.89	93.75	91.87	96.00
Fold 3	96.50	96.50	96.50	96.50
Fold 4	95.36	95.50	98.40	92.50
Average	94.75	94.75	94.98	94.60
Std Dev	1.10	1.16	2.66	1.57

Table S2. Performance of frame classification models across five folds.

Fold	F <sub>1</sub> -score (%)	Accuracy (%)	Precision (%)	Recall (%)
Fold 0	94.65	94.85	98.37	91.21
Fold 1	96.43	96.48	97.93	94.98
Fold 2	96.53	96.61	98.69	94.47
Fold 3	94.44	94.60	97.33	91.71
Fold 4	96.15	96.23	98.17	94.22
Average	95.64	95.75	98.10	93.32
Std Dev	0.94	0.88	0.49	1.39

validation, and testing sets with ratios of 0.8, 0.1, and 0.1, respectively. The average F1-score of the video storyboard classification models was  $94.75\% \pm 1.1$ . The results for each cross-validation fold are shown in Table S1.

#### B.2. Video Selection and Trimming

**Frame classification.** A ResNet18 [22] was trained for the surgical/non-surgical video frame classification task. To produce the annotations, the videos were sampled at one frame per second (fps). We annotated 7967 frames, 5481 of which turned to be surgical, and 2486, non-surgical.

**Video trimming.** Most online videos contain introductory and conclusion slides. Experimentally, we found that the start and end of the surgical footage can be reliably identified by finding the first and last three consecutive frames classified as surgical by our surgical frame classifier (sampling the video at 1 fps). Therefore, this is the approach we used to discard the non-surgical parts at the beginning and end of the collected videos. The resulting videos were manually quality controlled.

**Performance of frame classification models.** We trained five frame classification models to classify a video frame as either surgical or non-surgical. Each model of the five was trained in a different training-validation-testing split of the data, with a split rate of 0.8, 0.1, and 0.1. As shown in Table S2, the average F1-score of the frame classification models was  $95.64\% \pm 0.94$ .

You are a highly knowledgeable assistant specializing in surgical procedures and medical terminology.

Your expertise includes identifying and categorizing surgical interventions based on clinical descriptions and procedural contexts.

Here is a list of 35 possible surgical procedure types: pancreatotomy, pancreaticoduodenectomy, splenectomy, ampullectomy, hepatectomy, nephrectomy, low anterior resection, colectomy, abdominoperineal resection, pulmonary lobectomy, hartmanns, prostatectomy, gastric bypass, duodenal switch, gastrectomy, small bowel resection, hernia repair, ulcer repair, cholecystectomy, appendectomy, ileocolic resection, cecectomy, myomectomy, hysterectomy, nissen fundoplication, adrenalectomy, thymectomy, rectopexy, adhesiolysis, esophagectomy, cystectomy, jejunostomy, ileorectal anastomosis, kidney transplant, vaginectomy.

Based on the description of the surgical video: <video title>, determine the most likely procedure type from the list. Focus on matching the description to the procedure type that best aligns with the terminology and context provided.

Figure S1. ChatGPT prompt employed to match video titles to procedure types. The title of the video to be matched is inserted where the <video title> tag is located.

### B.3. Video Annotation

For the surgery type, a video is considered to be robotic if the video title includes any of the following keywords: *Robotic*, *Robot*, *Robo*, *Hugo*, *Versius*, *Senhance*, *Telerobotic*, *Console*, and *da Vinci*. The search for these terms in the video titles was case-insensitive. The remaining videos, with titles that do not include any of these keywords, are manually verified to ensure that they are manual surgical procedures. For the surgical procedure type, we cross-reference the video titles with the predefined list of procedures. When exact title matches are not found, we leverage the capabilities of the ChatGPTv4 API to perform a more nuanced analysis, incorporating a customized prompt as shown in Fig. S1. All annotations are manually quality controlled.

After curation, the final Surg-3M dataset resulted in 4194 surgical videos, 94% of which are  $1280 \times 720p$ , the remaining 6% have varied resolutions, with a minimum of  $640 \times 480$  pixels.

### C. SurgFM Pretraining: Implementation Details

This section provides an overview of the pretraining process for the SurgFM model, and the image preprocessing pipeline employed.

**SurgFM pretraining.** For the pretraining of SurgFM, we utilized eight NVIDIA V100 GPUs (32 GB) with a batch size of 24 per GPU. We employed AdamW as the optimizer with a teacher temperature of 0.04, fp16 precision, an initial learning rate of  $5e-4$  (after warm-up), and a minimum learning rate of  $1e-6$ . The model was trained for 60 epochs, including 10 warm-up epochs. This number of epochs enables the model to converge and stabilize its training loss on our dataset and pretext task. The model with the lowest

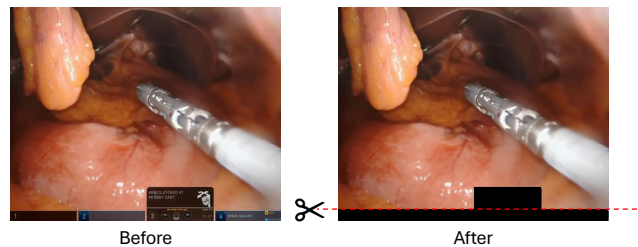


Figure S2. **Image preprocessing in SurgFM.** We automatically detect and crop out the user interface information from the surgical frames.

Table S3. Performance of bounding box detection models across five folds.

Fold	Images	Instances	Box Precision (%)	Box Recall (%)	mAP50 (%)	mAP50-95 (%)
Fold 0	272	447	74.79	77.63	75.50	62.00
Fold 1	272	438	70.73	77.40	76.36	61.79
Fold 2	272	509	83.34	79.60	84.89	68.56
Fold 3	272	422	75.27	83.69	80.31	68.98
Fold 4	272	496	81.32	81.45	82.58	68.65
Average	-	-	77.09	79.94	79.29	66.18
Std Dev	-	-	4.41	2.33	3.40	2.98

training loss was selected as the final model.

**Image preprocessing.** We utilize our trained non-surgical bounding-box detection model to identify and obliterate UI elements, as demonstrated in Fig. S2.

**Performance of non-surgical content detection models.** We trained five non-surgical content detection models to detect and obliterate *non-surgical* regions in *surgical* video frames. Each model was trained on a different training-validation-testing split of the data, with a split ratio of 0.8, 0.1, and 0.1, respectively. The average mAP50 of the five models was  $79.29\% \pm 3.4$ , and the average mAP50-95 was  $66.18\% \pm 2.98$ . The results for all the cross-validation folds are shown in Table S3.

## D. Downstream Tasks: Data Splits and Fine-tuning

In this section, we provide the details of the datasets used to evaluate each downstream task along with their corresponding data splits.

**Surgical phase recognition.** For M2CAI16, we follow the data splits in [26, 30, 54], dividing the dataset into 27 training videos and 14 testing videos, respectively. For Cholec80, we adopt the data splits in [12, 27, 35, 54], allocating 40 videos for training, eight for validation, and 32 for testing. For AutoLaparo, we follow the standard split of ten training videos, four for validation, and seven for testing [57]. For GraSP, we adopt the data splits specified in [4], with four videos for training, four for validation, and five for testing.

**Surgical tool presence detection.** The data splits for Cholec80 and GraSP are identical to those employed in the surgical phase recognition task.

**Surgical action recognition.** For CholecT50, we follow the standard 5-fold data splits as proposed in [42]. For SAR-RARP50 [48] we use its recommended split of 27 videos for training, 13 for validation, and 10 for testing.

**Fine-tuning on Downstream tasks.** We used the teacher model from SurgFM as our backbone and employed three different protocols for downstream task fine-tuning. The images were resized to  $448 \times 448$  for all downstream tasks. The downstream models with linear heads were trained with a batch size of 112, an initial learning rate (LR) of  $1e-4$ , the AdamW optimizer, and cross-entropy loss. An early stopping criterion was applied, stopping training after 10 epochs if the validation loss shows no improvement.

For the surgical tool presence detection tasks and the CholecT50 action recognition task, we used a linear head. For the surgical phase recognition tasks, we utilized a TCN [12] head and followed the two-stage training approach outlined in TeCNO [12]. In the first stage, we trained the backbone with a linear head to perform frame-wise classification without temporal context. Then, we employed the TCN head to incorporate temporal information of the extracted features for predictions. The default TCN configuration was used, consisting of two stages, each containing nine layers. The TCN head was trained using the Adam optimizer with an initial learning rate of  $5e-3$  for 70 epochs to ensure sufficient training. The checkpoint with the lowest validation loss was selected as the optimal checkpoint. For the SAR-RARP50 [48] action recognition task, we trained our model in two modes: *online*, where the SurgFM teacher model was used as backbone with a TCN head that could see only the information from previous frames; and *offline*, where the SurgFM teacher model was paired with an MS-TCN head [33] to incorporate both previous and future frame information for a fair comparison with the methods

in [48]. For the TCN head, we maintained the same model configuration and hyperparameters as in the surgical phase recognition tasks. For the MS-TCN head, we adopted a 3-stage, 11-layer configuration, following the basic model setup in [33]. The model was trained using the Adam optimizer with an initial learning rate of  $5e-4$  for 70 epochs.

**Data scaling.** In Sec. 6 of the manuscript, we present the results of the data scaling experiments. For each scale (10%, 25%, 50%), we conducted a 5-fold cross-validation, with each fold randomly selected from the training dataset. The model configurations and hyperparameters were kept consistent across different data scales using the same settings as those used for the full training dataset.

## E. Evaluation of SurgFM-Vid

To evaluate the performance of our video classifier, SurgFM-Vid, we have split the Surg-3M dataset by videos, with 3369 videos for training and 825 videos for testing. Our vanilla SurgFM was trained on all the Surg-3M frames, therefore, to evaluate the video classification performance fairly, we have trained a new SurgFM model from scratch using only the frames of the 3369 videos in the training set that are accessible to all other classifiers in the comparison (i.e., 2.6 million frames instead of the usual 3.3 million frames in Surg-3M).

## F. Dataset and Licensing

We adhere to the same practices as other datasets created from YouTube and various sources on the Web, such as ImageNet [13], Kinetics [9], YouTube-VIS [61], YouTube-8M [1], Insect-1M [41], Moments-in-Time [40], Tai-Chi-HD [51], HD-Villa-100M [60], and AVSpeech [15]. Specifically, we provide the code to download and generate the Surg-3M dataset, a list of links to the original YouTube videos, and the corresponding annotations. Researchers working in academic institutions can request direct access to the full Surg-3M dataset in LMDB format for non-commercial purposes. We will also provide an online form for the YouTube video authors to opt out of our Surg-3M dataset. The Surg-3M dataset is provided under the [Creative Commons Attribution 4.0 International \(CC BY 4.0\) license](https://creativecommons.org/licenses/by/4.0/).

## References

- [1] Sami Abu-El-Haija, Nisarg Kothari, Joonseok Lee, Paul Natsev, George Toderici, Balakrishnan Varadarajan, and Sudheendra Vijayanarasimhan. YouTube-8M: A Large-Scale Video Classification Benchmark. *ArXiv*, 2016. 4, 3
- [2] Ons Aouedi, Alessio Sacco, Kandaraj Piamrat, and Guido Marchetto. Handling Privacy-Sensitive Medical Data With Federated Learning: Challenges and Future Directions. *IEEE Journal of Biomedical and Health Informatics*, 27(2): 790–803, 2023. 1
- [3] Mahmoud Assran, Mathilde Caron, Ishan Misra, Piotr Bojanowski, Florian Bordes, Pascal Vincent, Armand Joulin, Mike Rabbat, and Nicolas Ballas. Masked Siamese Networks for Label-Efficient Learning. In *Computer Vision – ECCV 2022*, pages 456–473, Cham, 2022. Springer Nature Switzerland. 3
- [4] Nicolás Ayobi, Santiago Rodríguez, Alejandra Pérez, Isabela Hernández, Nicolás Aparicio, Eugénie Dessevres, Sebastián Peña, Jessica Santander, Juan Ignacio Caicedo, Nicolás Fernández, and Pablo Arbeláez. Pixel-Wise Recognition for Holistic Surgical Scene Understanding. *ArXiv*, 2024. 2, 6, 7, 3
- [5] Dominik Batić, Felix Holm, Ege Özsoy, Tobias Czempiel, and Nassir Navab. EndoViT: pretraining vision transformers on a large collection of endoscopic images. *International Journal of Computer Assisted Radiology and Surgery*, 19(6): 1085–1091, 2024. 3, 6, 7
- [6] Gedas Bertasius, Heng Wang, and Lorenzo Torresani. Is Space-Time Attention All You Need for Video Understanding? In *Proceedings of the International Conference on Machine Learning (ICML)*, 2021. 8
- [7] Mathilde Caron, Ishan Misra, Julien Mairal, Priya Goyal, Piotr Bojanowski, and Armand Joulin. Unsupervised learning of visual features by contrasting cluster assignments. In *Proceedings of the 34th International Conference on Neural Information Processing Systems*, Red Hook, NY, USA, 2020. Curran Associates Inc. 3
- [8] Mathilde Caron, Hugo Touvron, Ishan Misra, Herve Jegou, Julien Mairal, Piotr Bojanowski, and Armand Joulin. Emerging Properties in Self-Supervised Vision Transformers. In *2021 IEEE/CVF International Conference on Computer Vision (ICCV)*, pages 9630–9640. IEEE, 2021. 2, 3, 4, 5
- [9] Joao Carreira and Andrew Zisserman. Quo Vadis, Action Recognition? A New Model and the Kinetics Dataset. In *2017 IEEE Conference on Computer Vision and Pattern Recognition (CVPR)*, pages 4724–4733. IEEE, 2017. 4, 3
- [10] Ting Chen, Simon Kornblith, Mohammad Norouzi, and Geoffrey Hinton. A simple framework for contrastive learning of visual representations. In *Proceedings of the 37th International Conference on Machine Learning*. JMLR.org, 2020. 3
- [11] Xinlei Chen, Haoqi Fan, Ross Girshick, and Kaiming He. Improved Baselines with Momentum Contrastive Learning. *ArXiv*, 2020. 3
- [12] Tobias Czempiel, Magdalini Paschali, Matthias Keicher, Walter Simson, Hubertus Feussner, Seong Tae Kim, and Nassir Navab. TeCNO: Surgical Phase Recognition with Multi-stage Temporal Convolutional Networks. In *Medical Image Computing and Computer Assisted Intervention – MICCAI 2020*, pages 343–352, Cham, 2020. Springer International Publishing. 6, 7, 3
- [13] Jia Deng, Wei Dong, Richard Socher, Li-Jia Li, Kai Li, and Li Fei-Fei. ImageNet: A large-scale hierarchical image database. In *2009 IEEE Conference on Computer Vision and Pattern Recognition*, pages 248–255. IEEE, 2009. 4, 3
- [14] Alexey Dosovitskiy, Lucas Beyer, Alexander Kolesnikov, Dirk Weissenborn, Xiaohua Zhai, Thomas Unterthiner, Mostafa Dehghani, Matthias Minderer, Georg Heigold, Sylvain Gelly, Jakob Uszkoreit, and Neil Houlsby. An Image is Worth 16x16 Words: Transformers for Image Recognition at Scale. *ArXiv*, abs/2010.11929, 2020. 4, 5
- [15] Ariel Ephrat, Inbar Mosseri, Oran Lang, Tali Dekel, Kevin Wilson, Avinatan Hassidim, William T Freeman, and Michael Rubinstein. Looking to listen at the cocktail party: a speaker-independent audio-visual model for speech separation. *ACM Trans. Graph.*, 37(4), 2018. 4, 3
- [16] Yazan Abu Farha and Jurgen Gall. MS-TCN: Multi-Stage Temporal Convolutional Network for Action Segmentation. In *2019 IEEE/CVF Conference on Computer Vision and Pattern Recognition (CVPR)*, pages 3570–3579. IEEE, 2019. 7
- [17] Christoph Feichtenhofer, Haoqi Fan, Jitendra Malik, and Kaiming He. SlowFast Networks for Video Recognition. In *2019 IEEE/CVF International Conference on Computer Vision (ICCV)*, pages 6201–6210. IEEE, 2019. 6, 7, 8
- [18] Luis C. Garcia-Peraza-Herrera, Sebastien Ourselin, and Tom Vercauteren. VideoSum: A Python Library for Surgical Video Summarization. In *Conference on New Technologies for Computer and Robot Assisted Surgery*, 2023. 1
- [19] Andrew Gilbert, Maciej Marciniak, Cristobal Rodero, Pablo Lamata, Eigil Samset, and Kristin Mcleod. Generating Synthetic Labeled Data From Existing Anatomical Models: An Example With Echocardiography Segmentation. *IEEE Transactions on Medical Imaging*, 40(10):2783–2794, 2021. 1
- [20] Rohit Girdhar and Kristen Grauman. Anticipative Video Transformer. In *2021 IEEE/CVF International Conference on Computer Vision (ICCV)*, pages 13485–13495. IEEE, 2021. 6, 7
- [21] Guy Hacohen, Avihu Dekel, and Daphna Weinshall. Active Learning on a Budget: Opposite Strategies Suit High and Low Budgets. *ArXiv*, 2022. 5, 6
- [22] Kaiming He, Xiangyu Zhang, Shaoqing Ren, and Jian Sun. Deep Residual Learning for Image Recognition. In *2016 IEEE Conference on Computer Vision and Pattern Recognition (CVPR)*, pages 770–778. IEEE, 2016. 1
- [23] Kaiming He, Xinlei Chen, Saining Xie, Yanghao Li, Piotr Dollar, and Ross Girshick. Masked Autoencoders Are Scalable Vision Learners. In *2022 IEEE/CVF Conference on Computer Vision and Pattern Recognition (CVPR)*, pages 15979–15988. IEEE, 2022. 3, 4
- [24] Roy Hirsch, Mathilde Caron, Regev Cohen, Amir Livne, Ron Shapiro, Tomer Golany, Roman Goldenberg, Daniel Freedman, and Ehud Rivlin. Self-supervised Learning for Endoscopic Video Analysis. In *Medical Image Computing and Computer Assisted Intervention – MICCAI 2023*,

- pages 569–578, Cham, 2023. Springer Nature Switzerland. 3, 6, 7
- [25] Minh Hwang, Jeffrey Ichnowski, Brijen Thananjeyan, Daniel Seita, Samuel Paradis, Danyal Fer, Thomas Low, and Ken Goldberg. Automating Surgical Peg Transfer: Calibration With Deep Learning Can Exceed Speed, Accuracy, and Consistency of Humans. *IEEE Transactions on Automation Science and Engineering*, 20(2):909–922, 2023. 1
- [26] Yueming Jin, Qi Dou, Hao Chen, Lequan Yu, Jing Qin, Chi-Wing Fu, and Pheng-Ann Heng. SV-RCNet: Workflow Recognition From Surgical Videos Using Recurrent Convolutional Network. *IEEE Transactions on Medical Imaging*, 37(5):1114–1126, 2018. 6, 7, 3
- [27] Yueming Jin, Huaxia Li, Qi Dou, Hao Chen, Jing Qin, Chi-Wing Fu, and Pheng-Ann Heng. Multi-task recurrent convolutional network with correlation loss for surgical video analysis. *Medical Image Analysis*, 59:101572, 2020. 6, 7, 3
- [28] Yueming Jin, Yonghao Long, Cheng Chen, Zixu Zhao, Qi Dou, and Pheng-Ann Heng. Evaluation code from Temporal Memory Relation Network for Workflow Recognition From Surgical Video, 2021.
- [29] Yueming Jin, Yonghao Long, Cheng Chen, Zixu Zhao, Qi Dou, and Pheng-Ann Heng. Temporal Memory Relation Network for Workflow Recognition From Surgical Video. *IEEE Transactions on Medical Imaging*, 40(7):1911–1923, 2021. 6, 7
- [30] Yueming Jin, Yonghao Long, Xiaojie Gao, Danail Stoyanov, Qi Dou, and Pheng-Ann Heng. Trans-SVNet: hybrid embedding aggregation Transformer for surgical workflow analysis. *International Journal of Computer Assisted Radiology and Surgery*, 17(12):2193–2202, 2022. 6, 7, 3
- [31] Glenn Jocher, Ayush Chaurasia, and Jing Qiu. Ultralytics YOLO, 2023. 5
- [32] Kaidong Li, Mohammad I. Fathan, Krushi Patel, Tianxiao Zhang, Cuncong Zhong, Ajay Bansal, Amit Rastogi, Jean S. Wang, and Guanghui Wang. Colonoscopy polyp detection and classification: Dataset creation and comparative evaluations. *PLOS ONE*, 16(8):e0255809, 2021. 3
- [33] Shijie Li, Yazan Abu Farha, Yun Liu, Ming-Ming Cheng, and Juergen Gall. MS-TCN++: Multi-Stage Temporal Convolutional Network for Action Segmentation. *IEEE Transactions on Pattern Analysis and Machine Intelligence*, 45(6):6647–6658, 2023. 7, 3
- [34] Yanghao Li, Chao-Yuan Wu, Haoqi Fan, Karttikeya Mangalam, Bo Xiong, Jitendra Malik, and Christoph Feichtenhofer. MViTv2: Improved Multiscale Vision Transformers for Classification and Detection. In *2022 IEEE/CVF Conference on Computer Vision and Pattern Recognition (CVPR)*, pages 4794–4804. IEEE, 2022. 8
- [35] Yang Liu, Maxence Boels, Luis C. Garcia-Peraza-Herrera, Tom Vercauteren, Prokar Dasgupta, Alejandro Granados, and Sébastien Ourselin. LoViT: Long Video Transformer for surgical phase recognition. *Medical Image Analysis*, 99:103366, 2025. 6, 7, 8, 3
- [36] Zhuang Liu, Hanzi Mao, Chao-Yuan Wu, Christoph Feichtenhofer, Trevor Darrell, and Saining Xie. A ConvNet for the 2020s. In *2022 IEEE/CVF Conference on Computer Vision and Pattern Recognition (CVPR)*, pages 11966–11976. IEEE, 2022. 2, 5, 6, 7
- [37] Ze Liu, Jia Ning, Yue Cao, Yixuan Wei, Zheng Zhang, Stephen Lin, and Han Hu. Video Swin Transformer. In *2022 IEEE/CVF Conference on Computer Vision and Pattern Recognition (CVPR)*, pages 3192–3201. IEEE, 2022. 8
- [38] Lena Maier-Hein, Matthias Eisenmann, Duygu Sarikaya, Keno März, Toby Collins, Anand Malpani, Johannes Fallert, Hubertus Feussner, Stamatia Giannarou, Pietro Mascagni, Hirenkumar Nakawala, Adrian Park, Carla Pugh, Danail Stoyanov, Swaroop S. Vedula, Kevin Cleary, Gabor Fichtinger, Germain Forestier, Bernard Gibaud, Teodor Grantcharov, Makoto Hashizume, Doreen Heckmann-Nötzel, Hannes G. Kenngott, Ron Kikinis, Lars Mündermann, Nassir Navab, Sinan Onogur, Tobias Roß, Raphael Sznitman, Russell H. Taylor, Minu D. Tizabi, Martin Wagner, Gregory D. Hager, Thomas Neumuth, Nicolas Padoy, Justin Collins, Ines Gockel, Jan Goedeke, Daniel A. Hashimoto, Luc Joyeux, Kyle Lam, Daniel R. Leff, Amin Madani, Hani J. Marcus, Ozanan Meireles, Alexander Seitel, Dogu Teber, Frank Ückert, Beat P. Müller-Stich, Pierre Jannin, and Stefanie Speidel. Surgical data science – from concepts toward clinical translation. *Medical Image Analysis*, 76:102306, 2022. 1
- [39] Ozanan R Meireles, Guy Rosman, Maria S Altieri, Lawrence Carin, Gregory Hager, Amin Madani, Nicolas Padoy, Carla M Pugh, Patricia Sylla, Thomas M Ward, Daniel A Hashimoto, and the SAGES Video Annotation for A I Working Groups. SAGES consensus recommendations on an annotation framework for surgical video. *Surgical Endoscopy*, 35(9):4918–4929, 2021. 1
- [40] Mathew Monfort, Carl Vondrick, Aude Oliva, Alex Andonian, Bolei Zhou, Kandan Ramakrishnan, Sarah Adel Bargal, Tom Yan, Lisa Brown, Quanfu Fan, and Dan Gutfreund. Moments in Time Dataset: One Million Videos for Event Understanding. *IEEE Transactions on Pattern Analysis and Machine Intelligence*, 42(2):502–508, 2020. 4, 3
- [41] Hoang-Quan Nguyen, Thanh-Dat Truong, Xuan Bac Nguyen, Ashley Dowling, Xin Li, and Khoa Luu. Insect-Foundation: A Foundation Model and Large-Scale 1M Dataset for Visual Insect Understanding. In *2024 IEEE/CVF Conference on Computer Vision and Pattern Recognition (CVPR)*, pages 21945–21955. IEEE, 2024. 3
- [42] Chinedu Innocent Nwoye and Nicolas Padoy. Data Splits and Metrics for Method Benchmarking on Surgical Action Triplet Datasets. *ArXiv*, 2022. 5, 7, 3
- [43] Chinedu Innocent Nwoye, Cristians Gonzalez, Tong Yu, Pietro Mascagni, Didier Mutter, Jacques Marescaux, and Nicolas Padoy. Recognition of Instrument-Tissue Interactions in Endoscopic Videos via Action Triplets. In *Medical Image Computing and Computer Assisted Intervention – MICCAI 2020*, pages 364–374, Cham, 2020. Springer International Publishing. 6, 7
- [44] Chinedu Innocent Nwoye, Tong Yu, Cristians Gonzalez, Barbara Seeliger, Pietro Mascagni, Didier Mutter, Jacques Marescaux, and Nicolas Padoy. Rendezvous: Attention mechanisms for the recognition of surgical action triplets

- in endoscopic videos. *Medical Image Analysis*, 78:102433, 2022. 2, 4, 6, 7
- [45] Krystel Nyangoh Timoh, Arnaud Hualme, Kevin Cleary, Myra A Zaheer, Vincent Lavoué, Dan Donoho, and Pierre Jannin. A systematic review of annotation for surgical process model analysis in minimally invasive surgery based on video. *Surgical Endoscopy*, 37(6):4298–4314, 2023. 1
- [46] Maxime Oquab, Timothée Darcet, Théo Moutakanni, Huy Vo, Marc Szafraniec, Vasil Khalidov, Pierre Fernandez, Daniel Haziza, Francisco Massa, Alaaeldin El-Nouby, Mahmoud Assran, Nicolas Ballas, Wojciech Galuba, Russell Howes, Po-Yao Huang, Shang-Wen Li, Ishan Misra, Michael Rabbat, Vasu Sharma, Gabriel Synnaeve, Hu Xu, Hervé Jegou, Julien Mairal, Patrick Labatut, Armand Joulin, and Piotr Bojanowski. DINOv2: Learning Robust Visual Features without Supervision. *ArXiv*, 2023. 4
- [47] Nicolas Padoy, Deepak Alapatt, Jennifer Eckhoff, Daniel Hashimoto, Guy Rosman, Pietro Mascagni, Xiang Li, Ban Yutong, Sarah Choksi, Li Quanzheng, Filippo Filicori, Jean-Paul Mazellier, and Zhiliang Lyu. SAGES CVS Challenge (CVS-Challenge) - Grand Challenge, 2024. 2
- [48] Dimitrios Psychogyios, Emanuele Colleoni, Beatrice Van Amsterdam, Chih-Yang Li, Shu-Yu Huang, Yuchong Li, Fucang Jia, Baosheng Zou, Guotai Wang, Yang Liu, Maxence Boels, Jiayu Huo, Rachel Sparks, Prokar Dasgupta, Alejandro Granados, Sebastien Ourselin, Mengya Xu, An Wang, Yanan Wu, Long Bai, Hongliang Ren, Atsushi Yamada, Yuriko Harai, Yuto Ishikawa, Kazuyuki Hayashi, Jente Simoens, Pieter DeBacker, Francesco Cisternino, Gabriele Furnari, Alex Mottrie, Federica Ferraguti, Satoshi Kondo, Satoshi Kasai, Kousuke Hirasawa, Soohee Kim, Seung Hyun Lee, Kyu Eun Lee, Hyoun-Joong Kong, Kui Fu, Chao Li, Shan An, Stefanie Krell, Sebastian Bodenstedt, Nicolas Ayobi, Alejandra Perez, Santiago Rodriguez, Juanita Puentes, Pablo Arbelaez, Omid Mohareri, and Danail Stoyanov. SAR-RARP50: Segmentation of surgical instrumentation and Action Recognition on Robot-Assisted Radical Prostatectomy Challenge. *ArXiv*, 2023. 2, 4, 6, 7, 3
- [49] Sanat Ramesh, Vinkle Srivastav, Deepak Alapatt, Tong Yu, Aditya Murali, Luca Sestini, Chinedu Innocent Nwoye, Idris Hamoud, Saurav Sharma, Antoine Fleurentin, Georgios Exarchakis, Alexandros Karargyris, and Nicolas Padoy. Dissecting self-supervised learning methods for surgical computer vision. *Medical Image Analysis*, 88:102844, 2023. 2, 3, 4, 6, 7, 8
- [50] Tobias Rueckert, Daniel Rueckert, and Christoph Palm. Methods and datasets for segmentation of minimally invasive surgical instruments in endoscopic images and videos: A review of the state of the art. *Computers in Biology and Medicine*, 169:107929, 2024. 1
- [51] Aliaksandr Siarohin, Stéphane Lathuilière, Sergey Tulyakov, Elisa Ricci, and Nicu Sebe. First order motion model for image animation. In *Proceedings of the 33rd International Conference on Neural Information Processing Systems*. Curran Associates Inc., Red Hook, NY, USA, 2019. 3
- [52] G. E. Spoorthi, Subrahmanyam Gorthi, and Rama Krishna Sai Subrahmanyam Gorthi. PhaseNet: A Deep Convolutional Neural Network for Two-Dimensional Phase Unwrapping. *IEEE Signal Processing Letters*, 26(1):54–58, 2019. 6, 7
- [53] Ralf Stauder, Daniel Ostler, Michael Kranzfelder, Sebastian Koller, Hubertus Feußner, and Nassir Navab. The TUM LapChole dataset for the M2CAI 2016 workflow challenge. *ArXiv*, 2016. 2, 4, 6
- [54] Andru P. Twinanda, Sherif Shehata, Didier Mutter, Jacques Marescaux, Michel de Mathelin, and Nicolas Padoy. EndoNet: A Deep Architecture for Recognition Tasks on Laparoscopic Videos. *IEEE Transactions on Medical Imaging*, 36(1):86–97, 2017. 2, 3, 4, 5, 6, 7
- [55] Natalia Valderrama, Paola Ruiz Puentes, Isabela Hernández, Nicolás Ayobi, Mathilde Verlyck, Jessica Santander, Juan Caicedo, Nicolás Fernández, and Pablo Arbeláez. Towards Holistic Surgical Scene Understanding. In *Medical Image Computing and Computer Assisted Intervention – MICCAI 2022*, pages 442–452, Cham, 2022. Springer Nature Switzerland. 6, 7
- [56] Wenhai Wang, Enze Xie, Xiang Li, Deng-Ping Fan, Kaitao Song, Ding Liang, Tong Lu, Ping Luo, and Ling Shao. Pyramid Vision Transformer: A Versatile Backbone for Dense Prediction without Convolutions. In *2021 IEEE/CVF International Conference on Computer Vision (ICCV)*, pages 548–558. IEEE, 2021. 5
- [57] Ziyi Wang, Bo Lu, Yonghao Long, Fangxun Zhong, Tak-Hong Cheung, Qi Dou, and Yunhui Liu. AutoLaparo: A New Dataset of Integrated Multi-tasks for Image-guided Surgical Automation in Laparoscopic Hysterectomy. In *Medical Image Computing and Computer Assisted Intervention – MICCAI 2022*, pages 486–496, Cham, 2022. Springer Nature Switzerland. 2, 4, 6, 3
- [58] Zhao Wang, Chang Liu, Shaoting Zhang, and Qi Dou. Foundation Model for Endoscopy Video Analysis via Large-Scale Self-supervised Pre-train. In *Medical Image Computing and Computer Assisted Intervention – MICCAI 2023*, pages 101–111, Cham, 2023. Springer Nature Switzerland. 3
- [59] Thomas M Ward, Danyal M Fer, Yutong Ban, Guy Rosman, Ozanan R Meireles, and Daniel A Hashimoto. Challenges in surgical video annotation. *Computer Assisted Surgery*, 26(1):58–68, 2021. 1
- [60] Hongwei Xue, Tiankai Hang, Yanhong Zeng, Yuchong Sun, Bei Liu, Huan Yang, Jianlong Fu, and Baining Guo. Advancing High-Resolution Video-Language Representation with Large-Scale Video Transcriptions. In *2022 IEEE/CVF Conference on Computer Vision and Pattern Recognition (CVPR)*, pages 5026–5035. IEEE, 2022. 3
- [61] Linjie Yang, Yuchen Fan, and Ning Xu. Video Instance Segmentation. In *2019 IEEE/CVF International Conference on Computer Vision (ICCV)*, pages 5187–5196. IEEE, 2019. 4, 3
- [62] Fangqiu Yi and Tingting Jiang. Hard Frame Detection and Online Mapping for Surgical Phase Recognition. In *Medical Image Computing and Computer Assisted Intervention – MICCAI 2019*, pages 449–457, Cham, 2019. Springer International Publishing. 6, 7
- [63] Kun Yuan, Vinkle Srivastav, Nassir Navab, and Nicolas Padoy. HecVL: Hierarchical Video-Language Pretraining

for Zero-Shot Surgical Phase Recognition. In *Medical Image Computing and Computer Assisted Intervention – MICCAI 2024*, pages 306–316, Cham, 2024. Springer Nature Switzerland. [2](#)